A 2 m inelastic X-ray scattering spectrometer at CMC-XOR, Advanced Photon Source

J. P. Hill,[a] D. S. Coburn,[a] Y.-J. Kim,[a,b] T. Gog,[c]* D. M. Casa,[c] C. N. Kodituwakku[c,d] and H. Sinn[c]

[a]Department of Condensed Matter Physics and Material Science, Brookhaven National Laboratory, Upton, NY 11973, USA, [b]Department of Physics, University of Toronto, Ontario, Canada, [c]X-ray Science Division, Advanced Photon Source, Argonne National Laboratory, Argonne, IL 60439, USA, and [d]Department of Physics, Western Michigan University, Kalamazoo, MI 49008, USA.
E-mail: gog@aps.anl.gov

The design and commissioning of an inelastic X-ray scattering instrument at CMC-XOR at the Advanced Photon Source is reported. The instrument features a 2 m vertical-scattering arm with a novel counterweight design to reduce the twisting moment as the arm is moved in the scattering plane. A Ge(733) spherical analyzer was fabricated and an overall resolution of 118 meV (FWHM) was obtained with a Si(444) monochromator and a Si(111) pre-monochromator. Early results from a representative cuprate, La_2CuO_4, are reported.

1. Introduction

Driven by the advances of third-generation synchrotron sources and their application to a number of highly relevant current problems, the technique of inelastic X-ray scattering (IXS) is presently undergoing a rapid growth around the world. The spectrometers for these experiments may be divided into three broad classes based on resolution: those with very high resolution, typically a few meV, used mainly in the study of collective atomic motion; those with medium resolution, typically a few hundreds of meV, used mainly in the study of electronic excitations; and, finally, some with lower resolution, typically around ~1 eV, used for the study of broader features. The discovery of resonant enhancements in the hard X-ray inelastic cross section (Kau *et al.*, 1996) has allowed the IXS technique to be applied to the study of compounds containing heavy elements, particularly strongly correlated electron systems, including the high-T_c-related cuprates (Hill *et al.*, 1998; Abbamonte *et al.*, 1999; Hasan *et al.*, 2000, 2002; Kim *et al.*, 2002, 2004; Lu *et al.*, 2005), the manganites (Inami *et al.*, 2003; Grenier *et al.*, 2005) and nickelates (Shukla *et al.*, 2003). As a result, there has been a huge increase in the number of IXS experiments and a demand for ever-improving experimental facilities. Several new instruments have been commissioned in recent years, including at ID16 at the ESRF, France, and BL11XU and BL12XU at SPring-8, Japan. Each of these features a horizontal-scattering geometry.

Here we report the development of a new vertical-geometry momentum-resolved IXS spectrometer. The design features a number of novel elements to facilitate medium-energy-resolution resonant and non-resonant IXS experiments.

2. Spectrometer

The detailed design of the new IXS spectrometer was determined by a number of constraints, such as an analyzer-to-sample distance of 2 m to provide the desired resolution; a vertical-scattering geometry to minimize polarization losses and to accommodate conventional (elastic) scattering experiments on the same spectrometer; and mechanical stability in the sample–analyzer–detector alignment as the momentum transfer is varied.

Many of the existing instruments feature multiple analyzers. This approach provides a significant advantage when measuring isotropic systems such as liquids or powders for which only the absolute value of the momentum transfer is important. In such cases, data from multiple reciprocal space points can be taken simultaneously, significantly improving the throughput of the instrument. One example is the LERIX instrument (Fister *et al.*, 2006) which covers almost 180° in 2θ with analyzers. When studying excitations in single crystals at medium photon energies, as discussed here, it is important that data be taken along high-symmetry directions in reciprocal space, necessitating the capability to freely orient the sample and vary the scattering angle 2θ. Together with the vertical geometry, this led to the decision to use a single analyzer.

The overall conceptual design of the instrument is shown in Fig. 1. It is built around conventional Huber GmbH rotational stages. In particular, a Huber 512.1 Euler cradle provides
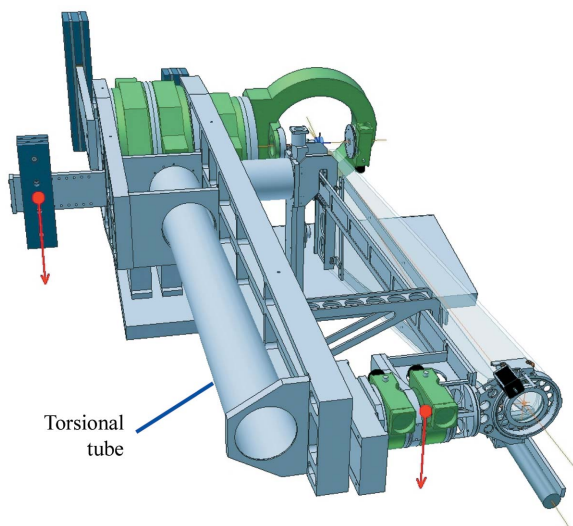
Figure 1
A downstream view of the 2 m IXS spectrometer designed for CMC-XOR, sector 9, Advanced Photon Source. The spectrometer features a 2 m vertical-scattering arm and a novel counterweight arrangement to eliminate twist in the scattering arm as the scattering angle is varied. The torsional tube is visible along the back of the 2θ arm. The forces corresponding to the weight of the counterweight and the analyzer circles are indicated by the arrows.

(χ, φ) degrees of freedom and a Huber 430 provides the θ rotation of the sample. The 2θ rotation is driven by two back-to-back Huber 440 stages. These provide both the large load-bearing capability required and additional stiffness for the 2 m 2θ arm. We discuss first the novel features of this 2θ arm.

Detailed finite-element analysis, performed using Algor software, showed that there was significant deformation of the arm owing to the loading resulting from the analyzer–detector combination and the flight tank. In particular, the effects of this load depend on the scattering angle, 2θ. When the arm is horizontal ($2\theta = 0°$) the load acts to supply a twisting torque to the arm, and when it is vertical ($2\theta = 90°$) the load acts to bend the arm out of the scattering plane.

Both deformations are of course undesirable, but twisting of the arm in particular would result in displacement of the analyzer along its vertical axis in the scattering plane. This translates into severe difficulties in keeping the analyzer at the same scattering angle as the arm moves in the scattering plane, making measurements with the desired energy resolution impractical.

In order to counteract the varying twisting torque, a novel counterweight system was designed. It uses a large torsional tube running down the rear side of the 2θ arm. This tube is rigidly welded to the analyzer end of the arm, but at the end closest to the center of rotation it passes through a large bearing. This tube, which is 152 mm in diameter and 3 mm thick, serves two functions. Firstly, it stiffens the 2θ arm to bending torques. Secondly, there is an adjustable horizontal counterweight of 37 kg on the end of this tube closest to the center of the instrument. This provides a torque that is transmitted through the bearing to the end of the 2θ arm. As the 2θ angle is varied, the torque provided by this counter-

weight also varies, from applying a twisting moment to applying a bending moment, in the same way as that provided by the weight of the analyzer–detector–flight-path combination. By varying the distance of the counterweight from the 2θ arm, the twisting moment provided by the weight of the analyzer, detector and flight-path can be countered.

Such an arrangement, when properly adjusted, should completely eliminate the twisting torque resulting from the movement of the 2θ arm in the vertical plane. Furthermore, by using the tube and bearing arrangement to place this counterweight close to the center of rotation, the total moment of the whole 2θ arm is minimized, and thus the required counterweight for the 2θ rotation itself is also minimized.

In order to determine the effectiveness of this system, tests were carried out to measure the twist of the 2θ arm. A laser was mounted on the arm at the analyzer position, and a position-sensitive detector was mounted at the sample position in the Euler cradle. Both θ and 2θ were moved the same amount so as to keep the laser and position-sensitive detector aligned. A perfectly rigid system would show no movement of the laser spot on the laser detector as the 2θ arm is rotated. Fig. 2 shows the results of this test as a function of 2θ. Here, vertical deviations represent a twist of the arm. A series of runs was performed for different positions of the counterweight. As can be seen, it is possible to adjust the counterweight such that the twist is minimized.

The figure also shows that total vertical deviation for the optimal counterweight position within $0° < 2\theta < 45°$ does not exceed 14 µm, corresponding to an angle deviation of 7 µrad for a 2 m arm.
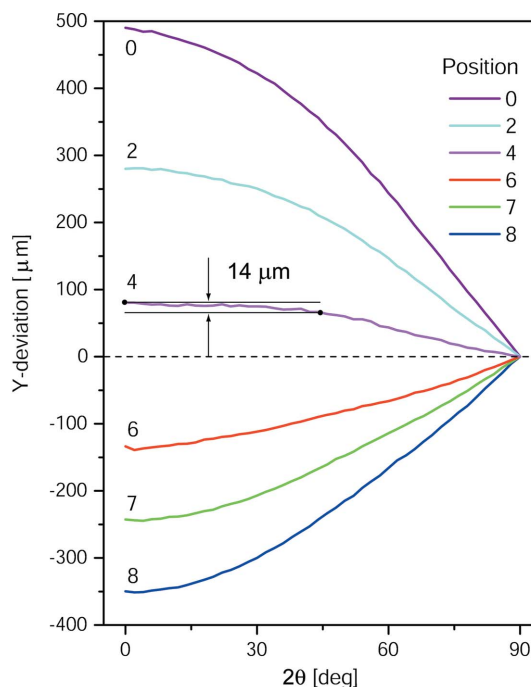
Figure 2
Twist of the 2θ arm for different counterweight positions ('0' is farthest from the arm) as a function of 2θ, indicated by the deviation of the analyzer position along its vertical axis. For the appropriate position, the effects of twist can be almost eliminated. The deviation indicated for position 4 is the maximum expected between $0° < 2\theta < 45°$.

Turning now to the rest of the spectrometer, the design incorporates a number of features to allow ease of use. These include modular analyzer mounts so that different analyzers are mounted in a frame that can be simply exchanged by means of a few thumbscrews. Also, both sample-to-analyzer and analyzer-to-detector distances are motorized and can be independently adjusted under computer control. The detector is an Amptek model XR-100CR solid-state detector, which provides 150 eV energy resolution, a maximum count rate of 10^4 counts s^{-1}, and a dark current of $\ll 1$ count min^{-1}. The active area is 3 mm in diameter, and there are a series of apertures that may be placed in front of the detector. These are again of a modular design and can be exchanged by undoing a single thumbscrew.

The detector itself is housed in a steel case, and a telescopic tube is adjusted to bridge the gap between the flight tank and the detector, reducing any possible air scatter into the detector. The flight tank is made of Plexiglas and has an adjustable telescoping 'snout' that may be extended close to the sample. The tank is filled with He gas. As a result of these measures, the background count rate is typically low: count rates of ≤ 1 count min^{-1} are routinely achievable.

In addition, a standard Bicron NaI scintillation detector is mounted on the flight tank looking at the sample at an angle from the scattered beam. This detector serves two functions. Firstly, it can be a point detector for measuring elastic scattering. This is particularly useful for finding Bragg reflections and for orienting a single-crystal sample. Secondly, it can be used as a fluorescence detector, for on-line energy calibration during the course of the experiment.

3. Analyzer

Monolithic curved analyzers suffer from strain broadening effects, compromising energy resolution. A common solution to this problem has been to dice the analyzer crystal into a large number of unstrained blocks, attached in some manner to a curved substrate. In this case the energy resolution results from the combined effects of the intrinsic resolution (the Darwin width) of the particular reflection and the geometrical effects arising from the finite block size, and the angular spread in the diffracted rays that impinge on a finite-sized detector as a result. The optimal balance between throughput and energy resolution is obtained when the source size (*i.e.* the portion of sample irradiated by the incident beam) is equal to the block size and the detector size (in the diffraction plane of the analyzer). Using Gaussian approximations for the apertures, Abbamonte (1999) has shown that the geometric contribution to the resolution, in a Rowland's circle geometry, is

$$(\Delta E)_{\text{geo}} = E \frac{\sqrt{3}}{2} \frac{\cos \theta_{\text{B}}}{\sin^2 \theta_{\text{B}}} \frac{D}{L}, \qquad (1)$$

where D is the block size, L is the distance from the sample to the analyzer and θ_{B} is the analyzer Bragg angle. This formula is more easily obtained by differentiation of Bragg's law and

replacing the angle differential by the block size divided by the Rowland's circle diameter $R = L \sin \theta_{\text{B}}$. The numerical factor is a result of approximating all apertures by Gaussian functions.

Thus, it appears from this equation that a block size as small as possible to minimize this contribution to the resolution is desirable. However, there are practical limits set by the finite-sized blade width of the dicing saw (typically $\sim$100 μm), which means that there is a large net loss of surface area for very small blocks, and a consequent loss of signal. Conversely, L can be increased to reduce this contribution; however, this also comes at the price of signal intensity because of the reduction in solid angle collected by the analyzer of a given size. In any case, the optimal size is determined by the source size as mentioned above.

The subject of the first experiments utilizing this instrument was resonant inelastic X-ray scattering at the Cu K-edge (8980.5 eV), with $\sim$100 meV resolution. For the analyzer, a Ge(733) reflection was chosen that had $\theta_{\text{B}} = 87.15°$ at the Cu K-edge.

The calculated instrument resolution is the intrinsic resolution added in quadrature to the geometrical contribution discussed above. For this reflection $(\Delta E)_{\text{intrinsic}} \simeq 50$ meV. A block size of 450 μm was chosen, giving an expected instrumental resolution of $[50^2 + 88^2]^{1/2} = 100$ meV at a radius of 2 m at the Cu K-edge.

It should be noted that the angular Darwin width for the chosen analyzer reflection is $\sim$100 μrad, or equivalent to just 200 μm vertical deviation owing to twisting. With this in consideration, the vertical deflections shown in Fig. 2 for counterweight positions other than optimal underline the importance of the anti-twist mechanism.

The analyzer was fabricated in-house in the following way. A 2 mm-thick 10 cm-diameter germanium (733) wafer was glued onto a 0.5 mm-thick 100 mm-diameter glass wafer using a low-viscosity epoxy glue (Epotek 301-2). A thin layer of glue was formed between the germanium and glass by placing a single droplet of glue in the center of the glass and then spreading it over the entire surface under moderate pressure. In this way, small dust particles are pushed to the edge of the wafer by the slowly propagating glue. Care was taken to ensure the final glue layer was both air-bubble- and dust-free. The epoxy was cured at 328 K for 12 h with 1.8 kg placed on top of the assembly. The average thickness of the glue after hardening was 8 μm.

The germanium wafer was then diced on a Kulicke and Soffa 984-10 Plus dicing machine. The cutting speed was 1 mm s^{-1} at a spindle speed of 20000 r.p.m. The width of the cuts was 100 μm and the pixel size was 450 μm × 850 μm. The depth of the cut was carefully controlled in order to cut only through the germanium and the glue without damaging the glass wafer.

The flat diced unit was then glued onto a concave glass mirror blank with a radius of 2 m using a similar gluing technique to that described above. To conform the analyzer to the sphere, a convex glass form with 1.98 m radius was pressed onto it with about 680 kg of weight during the hardening of the
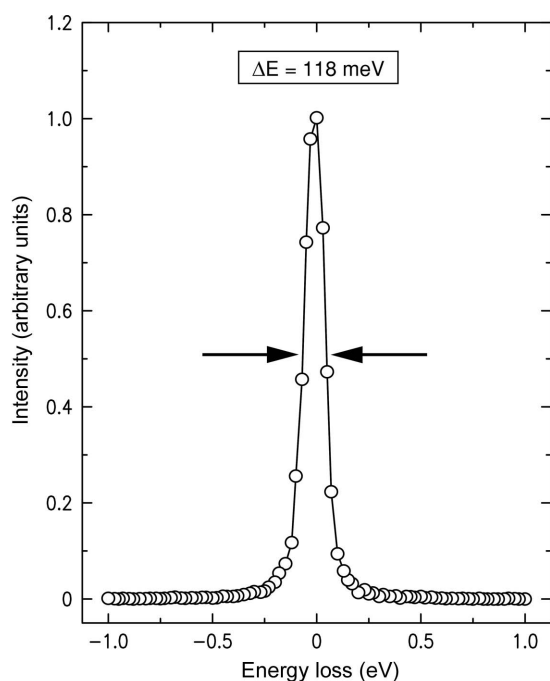
epoxy. A rubber pad was placed between the two to distribute the pressure uniformly.

In order to reduce the strain introduced by the dicing procedure, the analyzer was etched in 30% H_2O_2 solution at 338 K for about 1.5 h. About 20 µm of germanium was removed from the sides of each block in this process.

4. Performance of the instrument

In order to characterize the overall performance of the instrument, a piece of 3M scotch tape was used as a sample to provide a strong elastic signal. The monochromator consisted of a Si(111) liquid-nitrogen-cooled double-bounce pre-monochromator followed by a monolithic Si(444) double-bounce channel-cut crystal (Darwin width ~50 meV at the Cu K-edge). This set-up provides an incident flux of 5×10^{11} photons s^{-1} at 100 mA of stored ring current. The overall energy resolution of the instrument may then be obtained either by scanning both incident monochromators together and keeping the final energy fixed, or by scanning the analyzer and detector combination to change the outgoing energy, while keeping the incident energy fixed. Both scans were carried out by macro control within the *SPEC* diffractometer control software and produced identical results.

A representative scan is shown in Fig. 3. This was obtained with the incident slits in front of the pre-monochromator set to a gap of 0.4 mm, limiting the divergence of the beam incident on the monochromator to ~16 µrad, and a 0.5 mm aperture in front of the detector. The energy resolution thus obtained was 118 meV (FWHM), consistent with the calculated value of 100 meV. However, in placing successively smaller apertures
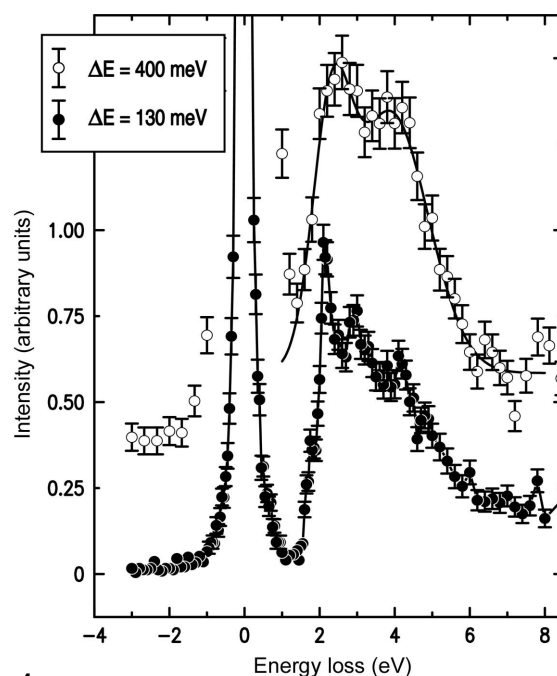
in front of the detector, it was clear that the focal spot size of the analyzer was not the optimum 0.9 mm, but perhaps a factor of two larger (this was also seen in optical measurements performed using diffuse laser light). While this does not compromise the ultimate resolution, which is defined by the detector aperture, it does translate into lost intensity and these results suggest that there is as much as a factor of two that can be gained in count rates by further improvements in the figure error of the spherical analyzer. Clearly, this would represent a significant gain for such an instrument and will be actively pursued in the next generation of analyzers.

4.1. Results on La₂CuO₄

In this section we report preliminary results taken on a prototypical cuprate, La_2CuO_4. This material has been studied in detail before (Kim *et al.*, 2002) and thus serves as a useful reference compound. Fig. 4 shows energy-loss scans taken at the peak of the resonant enhancement of the inelastic scattering, E_i = 8991 eV, with the momentum transfer set to the reciprocal lattice point (3,0,0) that is at the zone center. The earlier data, taken with a lower resolution configuration, are also shown [this set-up utilized a Si(333) monochromator and a R = 1 m Ge(733) analyzer with an overall resolution of 400 meV FWHM]. These earlier data were interpreted as possible evidence of two highly damped exciton-like modes (Kim *et al.*, 2002; Zhang & Ng, 1998). However, various alternative explanations were subsequently put forth (Tsutsui

Figure 3
Measured FWHM energy resolution of the instrument, with a Si(111) pre-monochromator, a Si(444) monochromator and a R = 2 m Ge(733) diced analyzer.

Figure 4
Energy-loss scans of La_2CuO_4 taken with the new instrument (filled circles) together with older data taken at 400 meV resolution in the same sample, at the same incident energy (empty circles). Data were taken at the (3,0,0) zone center wavevector with an incident energy of 8991 eV. Several new features are observed in the new data as a result of the improved resolution. The new data have a background of <1 count min^{-1} and a resolution of 130 meV. The data have been offset for clarity and scaled to have unit intensity.

et al., 1999; Nomura & Igarashi, 2005). The data taken with the new instrument (resolution 120 meV) reveal several new sharp features in the response that were not previously resolvable. It is hoped that the new level of detail provided by this instrument will help resolve the question as to which of the various theoretical approaches, if any, is the most appropriate description of the electronic excitations in this pivotal system.

It is clear that the improved resolution available at this instrument will be important in revealing new physics in these materials and it is anticipated that this will be a scientifically productive instrument for a number of years to come.

References

Abbamonte, P. (1999). PhD thesis, University of Illinois at Urbana-Champaign, USA.

Abbamonte, P., Burns, C. A., Isaacs, E. D., Platzman, P. M., Miller, L. L., Cheong, S. W. & Klein, M. V. (1999). *Phys. Rev. Lett.* **83**, 860–863.

Fister, T., Seidler, G., Wharton, L., Battle, A., Ellis, T., Cross, J., Macrander, A., Elam, W., Tyson, T. & Quian, Q. (2006). *Rev. Sci. Instrum.* **77**, 063901.

Grenier, S., Hill, J., Kiryukhin, V., Ku, W., Kim, Y.-J., Thomas, K., Cheong, S.-W., Tokura, Y., Tomioka, Y., Casa, D. & Gog, T. (2005). *Phys. Rev. Lett.* **94**, 047203.

Hasan, M., Montano, P., Isaacs, E., Shen, Z.-X., Eisaki, H., Sinha, S., Islam, Z., Motoyama, N. & Uchida, S. (2002). *Phys. Rev. Lett.* **88**, 177403.

Hasan, M. Z., Isaacs, E. D., Shen, Z.-X., Miller, L. L., Tsutsui, K., Tohyama, T. & Maekawa, S. (2000). *Science*, **288**, 1811–1814.

Hill, J., Kao, C.-C., Caliebe, W., Matsubara, M., Kotani, A., Peng, J. & Greene, R. (1998). *Phys. Rev. Lett.* **80**, 4967–4970.

Inami, T., Fukada, T., Mizuki, J., Ishihara, S., Kondo, H., Nakao, H., Matsumura, T., Hirota, K., Murakami, Y., Maekawa, S. & Endoh, Y. (2003). *Phys. Rev. B*, **67**, 045108.

Kao, C.-C., Caliebe, W., Hastings, J. & Gillet, J.-M. (1996). *Phys. Rev. B*, **54**, 16361–16364.

Kim, Y., Hill, J., Benthien, H., Essler, F., Jeckelmann, E., Choi, H., Noh, T., Motoyama, N., Kojima, K., Uchida, S., Casa, D. & Gog, T. (2004). *Phys. Rev. Lett.* **92**, 137402.

Kim, Y. J., Hill, J. P., Burns, C. A., Wakimoto, S., Birgeneau, R. J., Casa, D., Gog, T. & Venkataraman, C. T. (2002). *Phys. Rev. Lett.* **89**, 177003.

Lu, L., Chabot-Couture, G., Zhao, X., Hancock, J., Kaneko, N., Vajk, O., Yu, G., Grenier, S., Kim, Y., Casa, D., Gog, T. & Greven, M. (2005). *Phys. Rev. Lett.* **95**, 217003.

Nomura, T. & Igarashi, J. (2005). *Phys. Rev. B*, **71**, 035110.

Shukla, A., Rueff, J.-P., Badro, J., Vanko, G., Mattila, A., de Groot, F. & Sette, F. (2003). *Phys. Rev. B*, **67**, 081101.

Tsutsui, K., Tohyama, T. & Maekawa, S. (1999). *Phys. Rev. Lett.* **83**, 3705–3708.

Zhang, F. C. & Ng, K. K. (1998). *Phys. Rev. B*, **58**, 13520–13525.